Jurnal Akademika Kimia, 11(4): 202-210, November 2022
ISSN (online) 2477-5185 | ISSN (print) 2302-6030
http://jurnal.fkip.untad.ac.id/index.php/jak/

OPEN ACCESS

Synthesis and Characterisation of B-CDs/TiO_2 Composite

***Anthoni B. Aritonang, Uswatun Hasanah, Ajuk Sapar, Adhitiyawarman, & Puji Ardiningsih**
Program Studi Kimia/FMIPA – Universitas Tanjungpura, Pontianak – Indonesia 78124

Received 16 September 2022, Revised 10 October 2022, Accepted 01 November 2022
doi: 10.22487/j24775185.2022.v11.i4.pp202-210

Abstract

Synthesis of composite boron-doped carbon nanodots (B-CDs)/TiO_2 using the sol-gel method performed with titanium tetraisopropoxide (TTIP) precursor and B-CDs prepared by the microwave method using citric acid monohydrate, urea, and boric acid as precursors. The optimum concentration of boron dopant (B) on B-CDs/TiO_2 is 0.5% boron (w/w) which is then used as a composite on TiO_2 resulting in a brown solid and has blue luminescent under UV light. The result with UV-Vis/DRS for variation in B-CDs concentration of 0.5%, 1.25%, and 2.5% showed Eg values of 2.34 eV, 2.00 eV, and 2.29 eV. B-CDs cause the maximum emission peak (λEm) to redshift and affect the intensity of photoluminescence TiO_2. The characterization of FT-IR does not indicate a new peak, there is no bonding in the B-CDs/TiO_2 composite. The TiO_2 diffractogram was observed to shift towards a larger 2θ which caused the crystallinity of TiO_2 to decrease. Based on the photocatalytic activity test on the degradation of methylene blue solution, it showed fairly good activity. It is expected that the B-CDs/TiO_2 composite has the potential to be applied as a photocatalyst to degrade organic pollutants under visible light illumination.

Keywords: B-CDs, TiO_2, sol-gel, microwave, photoluminescence

Introduction

Semiconductor photocatalysts are smart materials that can be employed in the sterilization, air and water purification, and destruction of organic compounds processes. Titanium dioxide is a semiconductor that can be used (TiO_2). TiO_2 offers several advantages over other photocatalysts, including high efficiency, relatively cheap energy savings, non-toxicity, and no pollutant emissions (Lestari, 2017). There are three different types of TiO_2 crystal structures: rutile, anatase, and brookite. The anatase structure, with a band gap energy of 3.0-3.2 eV, is the TiO_2 structure that is frequently utilized (Linsebigler et al., 1995). TiO_2 is limited as a photocatalyst by its band gap, which with that much energy can only function under UV light (Aldrianti et al., 2020).

By introducing a buffer material, in this case, carbon nanodots (CDs), the efficiency of TiO_2 is boosted by lowering the band gap value so that its absorption can reach the visible light range. CDs are carbon-based substances that are classified as 0-dimension nanoparticle-sized carbon substances. Charge separation and the prevention of electron recombination are two effects that CDs composited on TiO_2 can have (Yao et al., 2008).

Syafei et al. (2017) reported on research into the synthesis of CDs/TiO_2 and how it can be utilized as a catalyst to break down chemicals that are persistent organic pollutants. Hydrothermal carbon quantum dots (CQDS)/TiO_2 have a better ability to degrade than titanium dioxide degussa (TiO_2-P25). Qu et al. (2013) created CQDs/TiO_2 doped with sulfur (S) and nitrogen (N) for the degradation of rhodamine B under visible light. N-doped CQDs/TiO_2 was created by Martins et al. (2016) and utilized to improve photocatalytic activity, decompose methylene blue, and change nitrogen (NO).

This study has used the sol-gel process to create boron carbon dots and titanium dioxide (B-CDs and TiO_2) (Syafei et al., 2017). The fundamental idea behind the sol-gel synthesis method is the creation of an initial component or precursor made of organic salts or organic metal compounds, followed by the polymerization of the solution to create the final product. Shen et al. (2021) novel visible light–driven carbon dot–TiO_2 nanosheet (CD-TN) photocatalysts are successfully prepared by loading CDs on the surface of TNs through the hydrothermal method. As expected, the removal efficiencies of CD-TNs for CR, RhB, and TC are

---

*Correspondence:
Anthoni B. Aritonang
e-mail: anthoni.b.aritonang@chemistry.untan.ac.id

94.6% (120 min), 97.2% (150 min), and 96.1% (60 min).

The first step was using the microwave method to prepare B-CDs. Microwave synthesis is sped up and made simpler by the use of microwaves. This approach is better than other methods for creating B-CDs since it is simple to use, non-toxic, inexpensive, and employs vibration to create a process that needs less energy (Hou et al., 2016).

It is anticipated that doping CDs with boron (B) will allow the photoluminescence (PL) spectrum to shift toward red (Ghifari et al., 2019). The concentration of the B-CDs employed in this investigation ranged from 0.5%, 1.25%, and 2.5% (w/w) B-CDs: (0.4 grams) TiO_2. B-CDs/TiO_2 was then evaluated using photoluminescence (PL), Fourier transforms infrared (FT-IR), ultraviolet-visible diffuse reflectance spectrophotometer (UV-Vis/DRS), and X-ray diffraction after being tested for success under a UV lamp at 365 nm (XRD).

This study sought to understand the features of B-CDs/TiO_2 composite produced using the sol-gel method, as well as the impact of these B-CDs on TiO_2, as well as the optimum concentration of B dopant on CDs using the microwave method.

Methods

The materials used in this study were: distilled water (H_2O), acetic acid (CH_3COOH; *Merck*), boric acid (H_3BO_3; *Merck*), citric acid monohydride ($C_6H_8O_7.H_2O$; *Merck*), acetylacetone ($C_5H_8O_2$; *Merck*), ethanol (C_2H_5OH 97 %; JT Baker), urea (CH_4N_2O; *Sigma Aldrich*) and titanium tetraisopropoxide (TTIP; 97%; *Sigma Aldrich*).

The equipment includes beakers, measuring cups, hotplates, condensers, three-neck flasks, magnetic stirrers, microwaves, ovens, droppers, measuring pipettes, volume pipettes, spatulas, and furnaces. The instruments include the Fourier transform infrared (FT-IR) Shimadzu IR prestige 21, photoluminescence spectrophotometer (PL) horrible FluoroMax 4, UVGL-55 Handheld UV Lamp 365 nm, ultraviolet-visible spectrophotometer (UV-Vis) Shimadzu UV-1280, ultraviolet-visible diffuse reflectance spectrophotometer (DR/UV-Vis) Agilent carry 60 and X-ray diffraction (XRD) X'Pert PRO PANalytical.

Preparation of B-CDs

50 mL of distilled water was added to 2 grams of citric acid, 4 grams of urea, and 3 grams of boric acid at concentrations of 0%, 0.5%, 1.5%, 2.5%, and 3.5% (w/w) each. The solution of citric acid, urea, and boric acid was swirled for 15 minutes using a magnetic stirrer before being heated in the microwave for 10 minutes. The obtained suspension was warmed in a 100 °C oven for 25 minutes. After that, the resulting B-CDs were examined with a 365 nm UV laser and described with UV-Vis, FT-IR, and PL.

Preparation of sol Ti(OH)n

Sol is created by combining the two solutions, I and II. 26.5 mL of ethanol, 2 mL of acetic acid, and 2 mL of distilled water were combined to create Solution I. 7.5 mL of TTIP was dissolved in 26.5 mL of ethanol to create Solution II. 1 mL of acetylacetone was added after Solution II had been introduced to a reflux flask and agitated with a magnetic stirrer. For two hours at 55 °C, the solution I was gradually added to solution II. To create a sol of Ti(OH)n, the solution was left to stand for 10 minutes. Poured into a container, the Ti(OH)n sol was then baked at 80 °C and calcined for three hours at 450 °C. The produced TiO_2 was examined using a UV lamp at 365 nm and studied with UV-Vis/DRS, FT-IR, XRD, and PL.

Preparation of B-CDs/TiO_2

By combining 0.4 grams of TiO_2 and B-CDs with concentration variations of 0.5%, 1.25%, and 2.5% (w/w), composites were created. After adding 5 mL of aquades, each mixture was agitated for 10 minutes. Dry for 12 hours in an oven set to 80 °C. B-CDs/TiO_2 were studied utilizing UV-Vis/DRS, FT-IR, XRD, and PL equipment after being seen under a 365 nm UV light.

Tools and materials

The equipment includes stir bars, spray bottles, bulbs, petri dishes, beakers, measuring cups, hotplates, condensers, three-neck flasks, magnetic stirrers, microwaves, ovens, droppers, measuring pipettes, volume pipettes, spatulas, and furnaces. The instruments include the Fourier transform infrared (FT-IR) Shimadzu IR prestige 21, photoluminescence spectrophotometer (PL) horiba FluoroMax 4, UVGL-55 Handheld UV Lamp 365 nm, ultraviolet-visible spectrophotometer (UV-Vis) Shimadzu UV-1280, ultraviolet-visible diffuse reflectance spectrophotometer (DR/UV-Vis) Agilent carry 60 and X-ray diffraction (XRD) X'Pert PRO PANalytical.

Results and Discussion

Synthesis of boron carbon nanodots (B-CDs)

Synthesis of the B-CDs/TiO_2 composite was carried out using the sol-gel method because it can produce a material with high homogeneity

The vibrational spectrum of a molecule, which serves to forecast the structure of chemical compounds, can be found using the FT-IR spectrum. **Figure 1** shows the results of the FT-IR instrument's characterization. According to **Figure 1**, the entire sample exhibits absorption at wave numbers between 3444 cm^{-1} and 3459 cm^{-1}, which corresponds to the stretching vibration of the OH group, specifically the carbonyl group and the NH group. The hydroxyl group present on the surface structure of CDs, designated as the C=O group, absorbs between wave numbers 1668 cm^{-1} and 1723 cm^{-1} (Bourlinos et al., 2015). The C=C group, which is the main component of CDs (Niu et al., 2014), is visible in the absorption region at wave numbers 1583 cm^{-1} to 1626 cm^{-1} (Pal et al., 2019). The CH group is indicated by the absorption area of wave number 1400 cm^{-1} - 1461 cm^{-1}, while the CN vibration is indicated by wave number 1150 cm^{-1} - 1118 cm^{-1} (Rahbar et al., 2019).

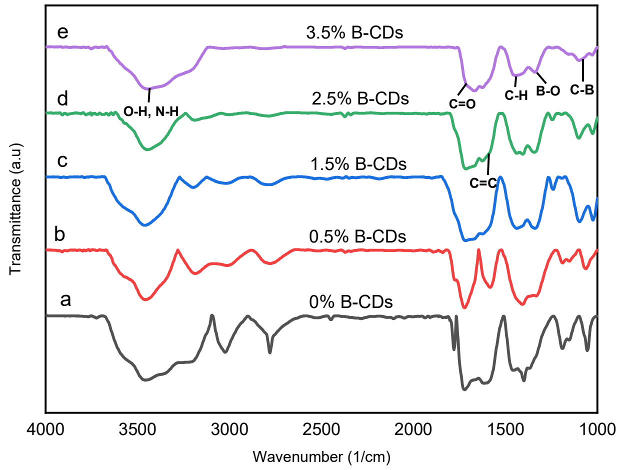

Figure 1. Spectrum FT-IR of 0% B-CDs (a), 0.5% B-CDs (b), 1.5% B-CDs (c), 2.5% B-CDs (d) and 3.5% B-CDs (e)

According to Vinayak et al. (2019), Bourlinos et al. (2015) & Pal et al. (2019), new absorptions at wave numbers 1031 cm^{-1} - 1450 cm^{-1} showing the BO group that appear due to stretching vibrations of BO_3 and/or BO_4 and are associated with the presence of boron in the structure of B-CDs and 1110 cm^{-1} - 1349 cm^{-1} showing a CB group that is an indication that boron has joined (Pal et al., 2019; Jia et al., 2019).

The CDs solution emits green luminescence when exposed to 365 nm UV light (Putro et al., 2019). while the B-CDs solution emits blue emission luminescence according to the research of Vinayak et al. (2019) which produces blue emission for the synthesis of boron-doped CDs using the microwave method.

To characterize B-CDs and identify their optical characteristics, such as their wavelength and band gap energy, a UV-Vis device was used. B-CDs absorb at a wavelength between 200 nm and 450 nm, which is in the UV and visible spectrum. The outcome based on **Figure 2** is a spectrum for B-CDs with two absorbance peaks. Due to the presence of aromatic C=C bonds in the B-CDs structure, the first peak, the π- π* transition, may be seen around the wavelength of 260 nm. The presence of C=O/BO bonds from different surface functional groups of B-CDs causes the second peak, an n- π* transition, to occur at a wavelength of 330 nm (Yan et al., 2018).

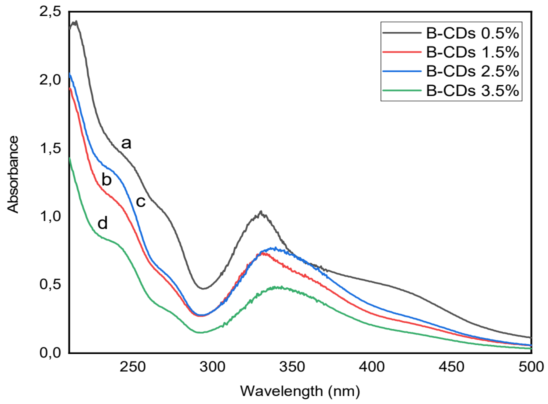

Figure 2. Spectrum Absorbance of 0.5% B-CDs (a), 1.5% B-CDs (b), 2.5% B-CDs (c) and 3.5% B-CDs (d)

Using the tauc plot method, the band gap energy of B-CDs is determined from the intersection of the peaks of a straight line drawn across the absorbance axis on the graph of the relationship between energy (eV) and $(\alpha h\upsilon)^{1/2}$. This is done by basing the calculation on the absorbance spectrum of the B-CDs.

Band gap energies of B-CDs produced with boron concentrations of 0%, 0.5%, 1.5%, 2.5%, and 3.5% are 2.52 eV, 2.50 eV, 2.78 eV, 2.52 eV, and 2.85 eV, respectively. Due to the quantum confinement effect of the B-CDs structure, which is a decrease in particle size dimensions that causes the energy levels to be different and causes the band gap energy to broadening, the band gap energy achieved at 1.5% and 3.5% boron concentrations is higher than that of 0% boron. band gap energy (Dewi et al., 2020). Band gap energy did not diminish at boron dopant concentrations of 1.5%, 2.5%, or 3.5%, showing that boron was just present at the surface and had no effect on the CDs structure (Luo et al., 2020).

The peak emission wavelength spectrum of CDs with variations in boron dopant concentration of 0%, 0.5%, 1.5%, 2.5%, and 3.5% (w/w) is calculated using PL characterization (**Figure 3**). In this investigation, the excitation wavelengths (λ_{Ex}) for the CDs sample, 0.5% sample, 1.5% sample, 2.5% sample, and 3.5% sample were 326 nm, 419 nm, and 360 nm, respectively. Different optical characteristics, emission sites, and B-CD sizes account for the various excitation wavelengths (λ_{Ex}) (Bao et al., 2011; Qu et al., 2012).

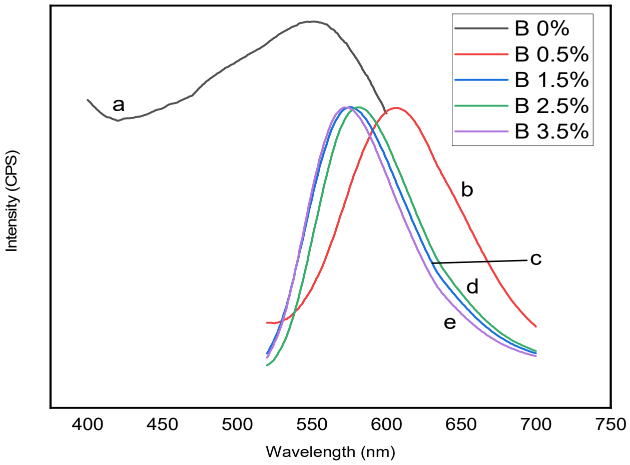

Figure 3. Spectrum Photoluminescence of 0% B-CDs (a), 0.5% B-CDs (b), 1.5% B-CDs (c), 2.5% B-CDs (d) and 3.5% B-CDs (d)

Due to the size distribution and single surface defect of the sp^2 on B-CDs, the addition of boron dopants on CDs tends to cause the peak of the PL spectrum to shift towards a larger wavelength and suffer an erratic reduction and increase in intensity (Li et al., 2012). The electrons in the sample B-CDs, which are in an unstable condition and will transition to a lower energy state, may be to blame for the reduction in the strength of the wave crest. With an increase in the amount of carbon in the colloid, which prevents all atoms from being able to excite, the change in the intensity of the wave crests indicates the existence of a quenching effect (Sadhanala & Nanda, 2016). The fluorescence spectrum was most effectively changed toward orange, which is closest to red, in CDs with 0.5% boron dopant concentration. The results of PL characterization agree with the results of characterization using a UV-Vis spectrophotometer.

Synthesis of B-CDs/TiO_2

In the prior technique, CDs with a concentration of 0.5% (the best outcome) were composited on TiO_2. B-CDs/TiO_2 is a solid that is dark brown. The surface of TiO_2 transfers electrons to B-CDs that are composited there. Charge separation, stability, and the prevention of electron recombination will all arise from this. The existence of holes created by free electrons in the B-CDs network can increase the amount of TiO_2 (Yao et al., 2008).

B-CDs were identified in the structure of B-CDs/TiO_2 by FT-IR characterization (**Figure 4**). The stretching vibration of the OH and NH groups, which has a wave number of 3441–3446 cm^{-1}, causes absorption throughout the entire material (Bourlinos et al., 2015). The OH bending vibration brought on by the absorption of water molecules is what causes the absorption at wave number 1635-1637 cm^{-1} (Zhang et al., 2016). The stretching vibration of Ti-O is absorbed in wave number 700-721 cm^{-1}. The lack of distinct absorbance peaks from TiO_2 such as C=O or CH_2 in samples of 0.5%, 1.25%, and 2.5% B-CDs/TiO_2 indicates that there are no chemical interactions between the TiO_2 composite and B-CDs (Syafei et al., 2017).

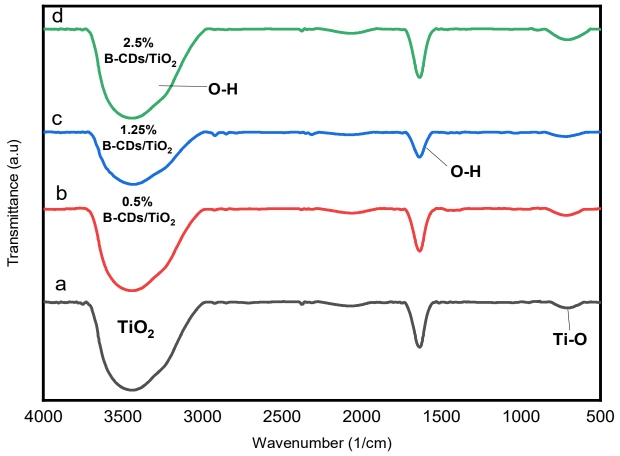

Figure 4. Spectrum FT-IR of TiO_2 (a), 0.5% B-CDs/TiO_2 (b), 1.25% B-CDs/TiO_2 (c) and 2.5% B-CDs/TiO_2 (d)

Under UV light at 365 nm, the luminescence characteristics of the B-CDs present in the colloidal solution of B-CDs/TiO_2 can be seen. TiO_2 emits a blue glow when combined with a concentration of B-CDs. TiO_2 causes a decrease in the photostability of B-CDs luminosity. As a result, the solution becomes more transparent as B-CD concentration is added. If B-CDs are evenly scattered in the water, the luminescence qualities will have better photostability. The solution photostability increases with increasing B-CDs content. B-CDs addition has an impact on TiO_2, although it cannot be noticed solely by visual inspection under a 365 nm UV lamp. The absorption wavelength of B-CDs/TiO_2 was therefore determined through characterization using UV-Vis/DRS spectrophotometer scans performed over 200-800 nm.

When TiO_2 with B-CDs was characterized, it was found that the absorption peak was observed in the visible light region with a wavelength of 400–800 nm rather than in the UV region with a wavelength of less than 400 nm (**Figure 5**). Increasing B-CDs concentration caused a longer shift, which suggests a shift in the direction of red. This shows that TiO_2 photocatalytic activity can be initiated in the region that absorbs visible light.

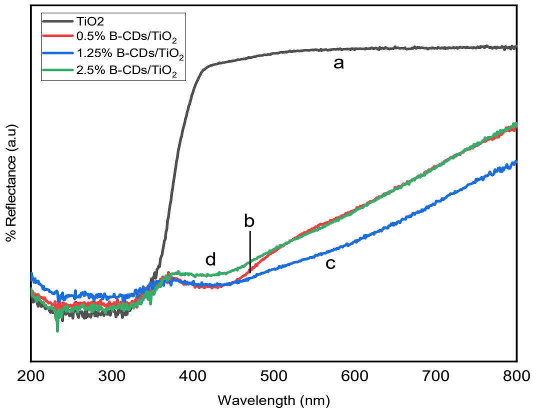

Figure 5. Spectrum DR-UV of TiO_2 (a), 0.5% B-CDs/TiO_2 (b), 1.25% B-CDs/TiO_2 (c) and 2.5% B-CDs/TiO_2 (d)

The band gap energy (Eg) was determined using the Kubelka-Munk equation:

$$F(R) = \frac{K}{S} = \frac{(1-R)^{1/n}}{2R} \quad (1)$$

In the equation, R is the percentage of the measured reflectance, K is the absorption coefficient, and S is the scattering coefficient. F(R) is the Kubelka-Munk factor. Using the Tauch formula, the Eg was determined (hυa) 1/n = A(hυ–Eg) (**Figure 6**). According to **Figure 6**, the band gap energy of the undoped TiO_2 was 3.27 eV, which is the same as the band gap energy of TiO_2 P25

Degussa. The band gap energy of TiO_2 in the anatase phase was 3.0-3.2 eV, which is also consistent with Linsebigler et al. (1995) assertion. TiO_2 band gap energy at 0.5% B-CDs concentration is 2.14 eV, and at 1.25% and 2.5%, it is 1.65 eV and 2.00 eV, respectively. When B-CDs is added as a dopant, the band gap energy of TiO_2 drops because the B-CDs cause the material to have more flaws, which lowers the band gap energy.

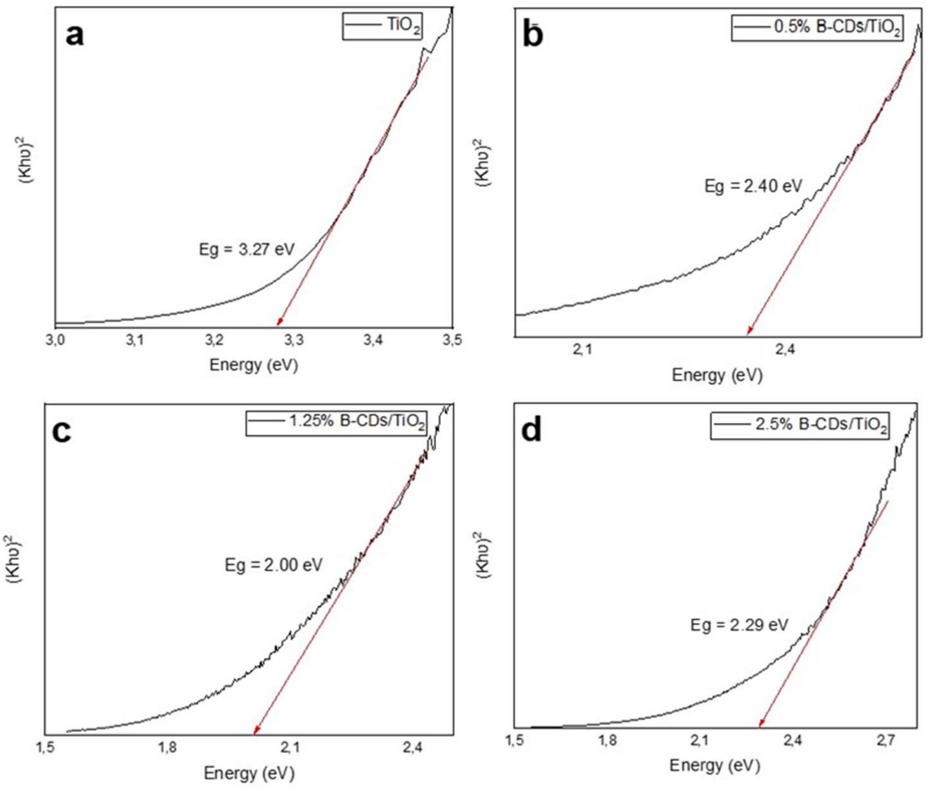

Figure 6. Band Gap of TiO_2 (a), 0.5% B-CDs/TiO_2 (b), 1.25% B-CDs/TiO_2 (c) and 2.5% B-CDs/TiO_2(d)

With the addition of 1.25% B-CDs concentration, the B-CDs/TiO_2 material had the lowest band gap energy. The energy needed to excite electrons from the valence band to the conduction band decreases as the band gap energy rises, and the generated particle size dimensions increase as well. The efficiency of the B-CDs/TiO_2 photocatalyst with changes in the concentration of B-CDs was then assessed using photoluminescence characterization.

Table 1. Maximum emission peak (λ_{Em}) and emission intensity of TiO_2 and B-CDs/TiO_2

Sample	λ_{Ex} (nm)	λ_{Em} (nm)	Intensity (CPS)
TiO_2	400	462	260850
0.5% B-CDs/TiO_2	352	436	3170730
1.25% B-CDs/TiO_2	432	524	1254580
2.5% B-CDs/TiO_2	352	433	1755770

Through PL research, the electron-hole pair recombination characteristics of a composite in the photocatalyst field can be investigated. Based on the observed PL emission spectrum, the outcomes of excited electron-hole pair recombination can be seen, and the effective charge carrier separation can be seen by the resulting PL intensity (Kavitha & Devi, 2014). According to **Table 1**, the addition of B-CDs to TiO_2 influences the photoluminescence intensity and causes the maximum emission peak

(λ_{Em}) for B-CDs/TiO_2 to shift towards a longer wavelength. **Table 1** displays the greatest emission peak (λ_{Em}) and emission intensity. When B-CDs are present, the photoluminescence of TiO_2 may be impacted, shifting the maximum emission peak (λ_{Em}) wavelength towards a longer one.

It was possible to determine the crystal phase, crystal size, and separation between TiO_2 and B-CDs/TiO_2 through analysis utilizing X-ray diffraction (XRD). Similarities can be seen in the three largest peaks of the diffractograms of TiO_2 and B-CDs/TiO_2 with various concentrations of B-CDs dopant, specifically in the range of 2θ 25°, 37°, and 48° (**Figure 7**).

According to JCPDS No. 00-021-1272, the three highest peaks that were formed indicated that the acquired TiO_2 had an anatase phase. It was clear that no new compound was produced from the B-CDs/TiO_2 based on the similarity of the diffraction angle peaks at TiO_2 and B-CDs/TiO_2. This demonstrates that B-CDs do not alter the TiO_2 crystal phase structure.

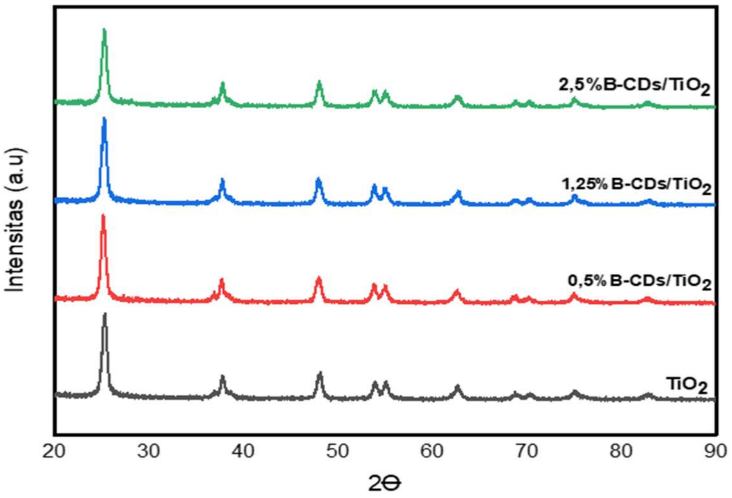

Figure 7. Diffractogram of TiO_2 (a), 0.5% B-CDs/TiO_2 (b), 1.25% B-CDs/TiO_2 (c) and 2.5% B-CDs/TiO_2 (d)

Table 2. 2θ diffraction angle, lattice distance, and crystallite size of TiO_2 and B-CDs/TiO_2

Material	2θ	d (nm)	D (nm)
TiO_2	25.277 37.663 47.984	0.260	38.822
0.5% B-CDs/TiO_2	25.272 37.774 47.918	0.259	42.160
1.25% B-CDs/TiO_2	25.252 37.778 48.014	0.259	36.652
25% SBCDs/TiO_2	25.413 37.819 48.088	0.258	34.553

According to **Table 2,** 0.5% B-CDs/TiO_2 has a typical peak of TiO_2 at 2θ 25.272°, 37.774°, and 47.918°. 1.25% B-CDs/TiO_2 at 2θ 25.252°, 37.778° and 48.014°. 2.5% B-CDs/TiO_2 at 2θ 25.413°, 37.819° and 48.088°. The 2θ shift is increased when B-CDs are added to TiO_2. The distance between the lattice (d) and the crystal size is increasing lower because B-CDs are comparatively amorphous (Syafei et al., 2017). The higher a material's photocatalytic abilities, the smaller its crystal size. **Table 2** shows the data for 2θ and d. Using the Debye-Scherrer equation, the three highest diffractogram peaks were used to calculate the crystallite size:

$$D = \frac{0.9\lambda}{\beta \cos \Theta}$$

D is the crystal firmness (crystal size) in nanometers (nm), k is the material constant with a value of <1 (the typical value is 0.9), λ is the wavelength of X-

(2)

rays used at the time of measurement (nm), B is the width of the half-peak on the diffractogram, and 2θ is determined from graph data 2θ on the diffractogram. Where is the x-ray wavelength (1,541), is the width half peak maximum (FWHM), and is the diffraction angle (degrees).

Conclusions

The optimum concentration of boron dopant in B-CDs is 0.5%, resulting in a band gap energy of 2.50 eV and a change in the photoluminescence spectrum that is most closely associated with the color red. A brown solid called B-CDs/TiO_2 glows blue when exposed to 365 nm UV light. The band gap energy value was obtained for the UV-Vis/DRS characteristics by adding 0.5% B-CDs/TiO_2 (2.00 eV), 1.25% B-CDs/TiO_2 (1.57 eV), and 2.5% B-CDs/TiO_2 (1.75 eV). The sample with the best value is produced by B-CDs with a boron concentration of 1.25% because B-CDs create a shift in the maximum emission peak in a bigger direction and alter the photoluminescence intensity of TiO_2. The limited surface stability of B-CDs on TiO_2 is shown by the fact that the FT-IR analysis did not reveal a different new absorption. As a sign that B-CDs were on the TiO_2 surface, the XRD characterization with TiO_2 diffractogram was seen to shift towards a bigger 2θ, which resulted in a decrease in the average crystallite size and a reduction in the distance between the lattices.

Acknowledgment

This work was supported by the research laboratory, Faculty of Mathematics and Natural Science, Tanjungpura University.

References

Aldrianti., Aritonang, A. B., & Syahbanu, I. (2020). Sintesis TiO_2/Ti terdoping logam Fe^{3+} menggunakan metode anodisasi dengan bantuan sinar tampak. *Jurnal Kimia Khatulistiwa, 8*(3), 45-52.

Bao, L., Liu, C., Zhang, Z., & Pang, D. (2015). Photoluminescence-tunable carbon nanodots: surface-state energy-gap tuning. *Advanced Materials*, *27*(10), 1663–1667.

Bourlinos, A. B., Trivizas, G., Karakassides, M. A., Baikousi, M., Kouloumpis, A., Gournis, D., Bakandritsos, A., Hola, K., Kozak, O., Zboril R., Papagiannouli, I., Alouskos, P., & Couris, S. (2015). Green and simple route toward boron doped carbon dots with significantly enhanced non-linear optical properties. *Carbon, 83*(March), 173-179.

Dewi, A. K., Aryanto, D., & Nurbaiti, U. (2020). Pengaruh perlakuan panas terhadap sifat optik lapisan tipis ZnO di atas ito. *Jurnal Fisika, 10*(1), 30-36.

Ghifari, A. D. A., Sanjaya, E., & Isnaeni. (2019). Pengaruh doping nitrogen, sulfur, dan boron terhadap spektrum absorbansi dan fotoluminesensi karbon dot asam sitrat. *Al-Fiziya Journal of Materials Science, Geophysics, Instrumentation and Theoretical Physics, 2*(2), 93-101.

Hou, J., Li, H., Wang, L., Zhang, P., Zhou, T., Ding, H., & Ding, L. (2016). Rapid microwave-assited synthesis of molecularly imprinted polymers on carbon quantum dots for fluorescent sensing of tetracycline in milk. *Talanta, 146*(January), 34-40.

Jia, Y., Hu, Y., Li, Y., Zeng, Q., Jiang, X., & Cheng, Z. (2019). Boron doped carbon dots as a multifunctional fluorescent probe for sorbate and vitamin B12. *Microchimica Acta, 186*(84), 1-10.

Kavitha, R & Devi, L. G. (2014). Synergistic effect between carbon dopant in titania lattice and surface carbonaceous species for enchanching the visible light photocatalysis. *Journal of Enviromental Chemical Engineering, 2*(2), 857-867.

Lestari, I. (2017). Degradasi senyawa organik pada palm oil mill secondary effluent menggunakan fotokatalis TiO_2. *Jurnal Citra Widya Edukasi, 9*(2), 143-152.

Li, Y., Zhao, Y., Cheng, H., Hu, Y., Shi, G., Dai, L., & Qu, L. (2012). Nitrogen-doped graphene quantum dots with oxygen-rich functional groups. *Journal of The American Chemical Society, 134*(1), 15-18.

Linsebigler, A. L., Lu, G., & Yates, J. T. (1995). Photocatalysis on TiO_2 surfaces: Prinsiples, mechanisms, and selected results. *Chemical Reviews, 95*(3), 735-758.

Luo, H., Dimitrov, S., Daboezi, M., Kim, J., Guo, Q., Fang, Y., Stoeckel, M., Samori, P., Fenwick, O., Sobrido, A. B. J., Wang, X., & Titirici, M. (2020). Nitrogen-doped carbon dots/TiO_2 nanoparticle composites for photoelectrochemical water oxidations. *American Chemical Society Applied Nano Materials, 3*(March), 3371-3381.

Martins, N. C. T., Ângelo J., Girão, A. V., Trindade, T., Andrade, L., & Mendes, A. (2016). N-doped carbon quantum dots/TiO_2 composite with improved photocatalytic activity. *Applied Catalysis B: Environmental, 192*(September), 67-74.

Niu, J., Gao, H., Wang, L., Xin, S., Zhang, G., Wang, Q., Guo, L., Liu, W., Gao, X., & Wang, Y. (2014). Facile synthesis and optical properties of nitrogen doped carbon dots. *New Journal of Chemistry*, *38*(4), 1522-1527.

Pal, A., Ahmad, K., Dutta, D., & Chattopadhyay, A. (2019). Boron doped carbon dots with unusually high photoluminescence quantum yield for ratiometric intracelluler pH sensing. *A European Journal Chemphyschem of Chemical Physics and Physical Chemistry, 20*(8), 1018-1027.

Putro, P. A., Roza, L., & Isnaeni. (2019). Karakterisasi sifat optik c-dots dari kulit luar singkong menggunakan teknik microwave. *Jurnal Teknologi Technoscientia,11*(2), 128-136.

Qu, D., Zheng, M., Du, P., Zhou, Y., Zhang, L., Li, D., Tan, H., Zhao., Xie, Z., & Sun, Z. (2013). Highly luminescent s, n co-doped graphene quantum dots with broad visible absorption bands for visible light photocatalysts. *Nanoscale, 5*(24), 12272-12277.

Qu, S., Wang, X., Lu, Q., Liu, X., & Wang, L. (2012). A biocompatible fluorescent ink based on water-soluble luminescent carbon nanodots. *Angewandte International Edition Chemie, 51*(49), 12215-12218.

Rahbar, M., Mehrzad, M., Behpour, M., Mohammadi-Aghdam, S., & Ashrafi, M. (2019). S, n co-doped carbon quantum dots/TiO_2 nanocomposite as highly efficient visible light photocatalyst. *Nanotechnology, 30*(September), 1-16.

Sadhanala, H. K., & Nanda, K. K. (2016). Boron doped carbon nanoparticles: Size-independent color tunability from red to blue and bioimaging applications. *Carbon, 96*(January), 166–173.

Shen, S., Li, R., Wang, H., & Fu, J. (2021). Carbon dot–doped titanium dioxide sheets for the efficient photocatalytic performance of refractory pollutants. *Frontier in Chemistry, 9*(September), 1-10.

Syafei, D., Sugiarti, S., Darmawan, N., & Khotib, M. (2017). Synthesis of TiO_2/carbon nanoparticle (C-dot) composites as active catalysts. *Indonesia Journal of Chemistry, 17*(1), 37-42.

Vinayak, Khan, F., Dewangan, P. K., & Chandra, C. (2019). Bovine serum albumin loaded boron doped carbon dots as a sensing probe for the detection of Pb(II) ion in water samples. *International Journal of Basic and Applied Research, 9*(3), 162-168.

Yan, Y., Chen, J., Li, N., Tian, J., Li, K., Jiang, J., Tian, Q., & Chen, P. (2018). Systematic bandgap engineering of graphene quantum dots and applications for photocatalytic water splitting and CO_2 reduction. *American Chemical Society Nano, 12*(March), 3523–3532.

Yao, Y., Li, G., Ciston, S., Lueptow, R. M., & Gray, K. A. (2008). Photoreactive TiO_2/carbon nanotube composites: Synthesis and reactivity. *Environmental Science & Technology, 42*(13), 4952–4957.

Zhang, Y., Liu, X., Fan, Y., Guo, X., Zhou, L., Lv, Y., & Lin, J. (2016). One-step microwave synthesis of n-doped hydroxyl functionalized carbon dots with ultra-high fluorescence quantum yields. *Nanoscale, 8*(33), 15281–15287.